

Magnetic shear-flows in stars

Rainer Arlt

Astrophysikalisches Institut Potsdam, An der Sternwarte 16, D-14482 Potsdam, Germany

Abstract. Many main-sequence stars exhibit extensive radiative zones. These may rotate differentially and have large-scale meridional circulations, while the solar radiative core rotates rigidly. We are concerned with three topics: The generation of magnetic fields by a dynamo effect of these large-scale motions, the stability of differential rotation if magnetic fields are present initially, and the formation of the solar tachocline being a thin transition layer from rigid solar core rotation to differential rotation of the outer convective shell. We conclude that dynamo-generation of magnetic fields is unlikely in stellar radiative envelopes. This finding supports the view that the fields of magnetic Ap stars are fossil. If they do exist from the beginning of the stellar life, they will make a differential rotation unstable if the angular velocity decreases with axis distance. This is the magneto-rotational instability. It is found that the time-scale of turning a differential rotation into a rigid one is about 10–100 million years. In the solar radiative core, the angular velocity gradient is positive and the magneto-rotational instability is not found. Nevertheless, magnetic fields will suppress differential rotation by the Lorentz force and reduce the transition between the differentially rotating convection zone and the core to a very thin layer. The field strength of the poloidal core magnetic field has to be of the order of 10 G in order to produce the solar tachocline thickness.

STELLAR DIFFERENTIAL ROTATION

There are several reasons why stars do not rotate like rigid bodies, but exhibit a differential rotation. The angular velocity may have latitudinal as well as radial gradients, and it depends on the origin of differential rotation which of the two dominates. One of the reasons is convection which turns a rigid rotation into a differential one. We are not concerned with this effect here; we will deal with those parts of stars which are not convective. These radiative zones are dynamically quiet and can be studied by means of numerical MHD simulations.

The Sun has a convective shell extending from the visible surface down to $0.71R_{\odot}$ (solar radii). Convection builds up a latitudinal gradient in the angular velocity. The pole rotates about 30% slower than the equator. Below $0.65R_{\odot}$, the solar core rotates rigidly. No significant deviations from rigid rotation are hitherto found in the solar core rotation. The region where differential rotation changes into a rigid one extends from roughly $0.65R_{\odot}$ to $0.72R_{\odot}$ (see e.g. [1]) and exhibits strong radial angular velocity gradients. It is termed ‘tachocline’.

Stars more massive than the Sun evolve differently. During most of their life-time, they possess a very small convective core up to $0.2R_{*}$ (stellar radii) and a huge envelope through which energy is transported by radiation instead of convection. Again, this is the region of interest. The convective core will impose differential rotation, now at the bottom of the envelope. Stars with masses of up to at least 2 solar masses went through a fully convective phase in their early life. There was an accretion disk around protostars

which couples to the star by magnetic fields and provides a rotational locking of the disk to the *surface* of the stars. Fully convective phase and disk coupling have left behind a star which rotates differentially even in its radiative envelope.

The final reason for differential rotation results from the angular momentum transport by the radiation itself [2]. The effect builds up a radial gradient of the angular velocity. Meridional flows start to compensate this gradient and the stationary-flow solution is an angular velocity profile depending on both radius and latitude plus a meridional circulation.

Given these configurations, we are interested in the following questions: (i) How does the tachocline form and what confines it to cover only a few per cent of the solar radius? (ii) Which of these flows are subject to the magnetorotational instability, and what is the evolution of differential rotation and magnetic fields? (iii) Are the large-scale flows in radiative shells capable of driving a dynamo? While the first two questions assume the presence of a measurable magnetic field from the beginning, the last question deals with the generation of magnetic fields if initial field strengths were very small.

FORMATION OF THE SOLAR TACHOCLINE

The effect of an initial poloidal magnetic field on the evolution of the internal rotation of radiative zones is studied with the spherical numerical code by Hollerbach [3]. The radiative zone studied in this Section is the solar core extending to the bottom of the convection zone at $0.71R_{\odot}$. The question of whether an internal poloidal magnetic field make the solar core rotate uniformly and at which field strengths, has been studied without meridional flows in [4] and [5]. The full 2D flow was computed by [6] and [7].

The code integrates the incompressible MHD equations in Boussinesq approximation, that is eliminating sound waves but including the effect of density fluctuations in a buoyancy force. In this approximation, density and temperature fluctuations are uniquely related. The non-dimensional equations read

$$\left(\frac{\partial}{\partial t} + \mathbf{u} \cdot \nabla\right) \mathbf{u} = \text{Pm} \nabla^2 \mathbf{u} - \nabla p + (\nabla \times \mathbf{B}) \times \mathbf{B} + \text{Ra}_{\eta} \theta \mathbf{r} \quad (1)$$

$$\frac{\partial \mathbf{B}}{\partial t} = \nabla^2 \mathbf{B} + \nabla \times (\mathbf{u} \times \mathbf{B}) \quad (2)$$

$$\left(\frac{\partial}{\partial t} + \mathbf{u} \cdot \nabla\right) \theta = \frac{\text{Pm}}{\text{Pr}} \nabla^2 \theta - u_r \frac{\partial T}{\partial r}, \quad (3)$$

where \mathbf{u} , \mathbf{B} , p and θ mean dimensionless velocity, magnetic field, pressure, and temperature fluctuation, respectively. All physical quantities are normalized with the magnetic diffusivity η , such as $t = R^2 \hat{t} / \eta$, $u = \eta \hat{u} / R$, and $B = \sqrt{\mu \rho} \eta \hat{B} / R$ where the hats denote variables with physical units. The momentum-equation thus involves the ratio of kinematic to magnetic diffusivity, $\text{Pm} = \nu / \eta$. The background temperature profile is an adiabatic one resulting from a shell heated from the bottom and is denoted by T . We will use these equations also in the following sections.

For the tachocline problem, it is assumed that the convection zone maintains a fixed angular velocity gradient at the outer boundary of the computational domain. The solar-

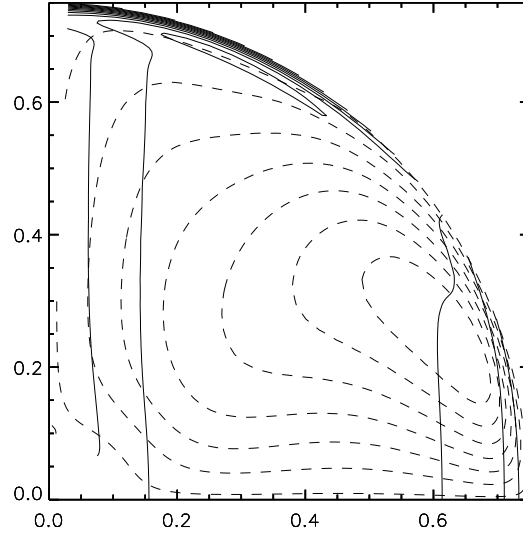


FIGURE 1. Vertical cross-section of the steady-state solution of the tachocline problem in the northern hemisphere of the solar radiative core. The solid lines represent isorotation, the dashed lines are contours of B_ϕ .

like differential rotation profile $\Omega(\theta) = \text{Rm}(1 - 0.13 \cos^2 \theta - 0.16 \cos^4 \theta)$ is used as a boundary condition, where $\text{Rm} = R\Omega_0/\eta$ is another parameter in the system. The initial velocity field inside the computational domain matches this boundary condition and depends only on the axis distance $s = r \sin \theta$ minimizing meridional circulations solely due to the rotation. The initial magnetic field is a poloidal one and is expressed by

$$B = \left(\frac{1}{r^2 \sin \theta} \frac{\partial A}{\partial \theta}, -\frac{1}{r \sin \theta} \frac{\partial A}{\partial r}, 0 \right) \text{ with } A = B_0 r^2 \left(1 - \frac{r}{r_o} \right) \left(1 - \frac{r_i}{r} \right) \sin^2 \theta \quad (4)$$

The radii r_i and r_o are the inner and outer boundaries of the computational domain; B_0 is the initial field strength and is a free parameter. Since the numerical system will be far more diffusive than the real plasma, this poloidal field is not evolved imitating the very long diffusive time-scale of more than 10^{10} yr in the Sun. The tachocline evolution is solved as an axisymmetric problem.

The system evolves into a steady-state solution in which the magnetic field has greatly reduced the volume in which differential rotation is significant. A thin tachocline-like layer is formed near the outer boundary as shown in Fig. 1. Since solar magnetic Reynolds numbers cannot be reached in a full numerical simulation, several runs at various Rm must be used for an extrapolation. It is found that an initial field strength of the poloidal magnetic field of $B_0 \sim 10$ G is sufficient for the formation of the tachocline.

MAGNETOROTATIONAL INSTABILITY IN STARS

The combination of a weak magnetic field and an angular-velocity profile decreasing with axis distance gives rise to an instability [8] which has been re-discovered in 1991

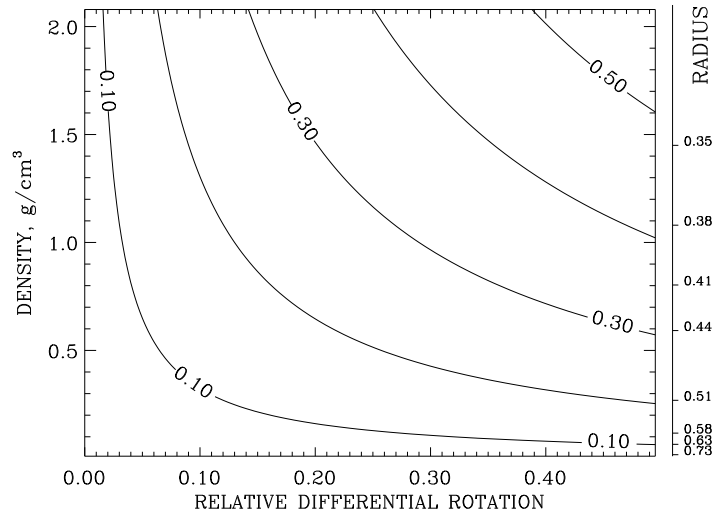


FIGURE 2. Minimum magnetic field in Gauss for an A star envelope depending on differential rotation and density. For larger field strengths, the growth rate of the MRI will dominate the diffusive decay rate.

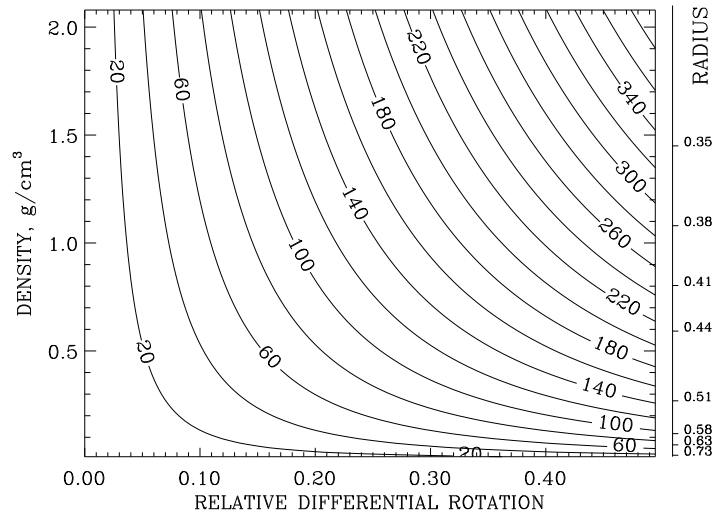


FIGURE 3. Maximum magnetic field in kG for an A star envelope depending on differential rotation and density. With stronger fields, the MRI will develop at highly reduced growth rates.

([9] and a series of follow-up papers). There is no lower limit for the magnetic field strength in ideal MHD. The lower limit for the field is set by the magnetic diffusivity which is very small in the fully-ionized gas in stellar radiative shells. Based on the relation between Temperature and magnetic diffusivity [10] the minimum is plotted as a function of density and differential rotation in Fig. 2.

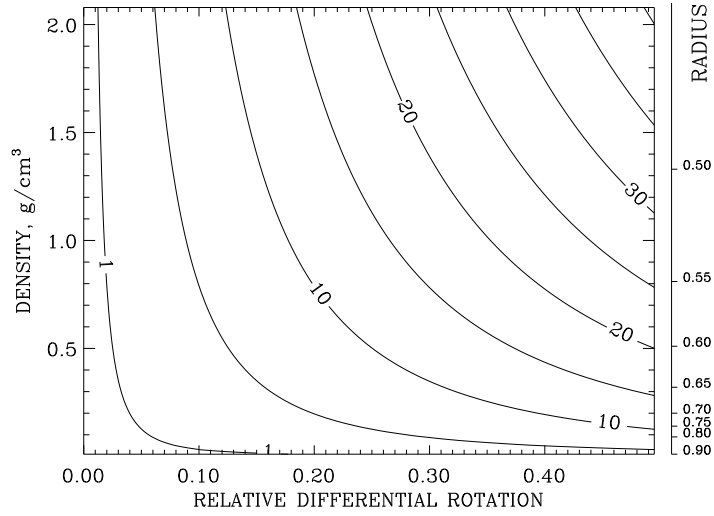


FIGURE 4. Maximum magnetic field in kG for the solar radiative interior depending on differential rotation and density.

The analysis of the MRI in the Boussinesq approximation shows that the fastest growing mode occurs when

$$(\mathbf{k} \cdot \mathbf{u}_A)^2 = -\frac{1}{4} \left(1 + \frac{\kappa^2}{4\Omega^2} \right) \frac{d\Omega^2}{d \ln R}, \quad (5)$$

where \mathbf{k} is the vector of the perturbation mode, \mathbf{u}_A is the Alfvén speed at a given magnetic field, $\mathbf{u}_A = \mathbf{B}/\sqrt{\mu\rho}$, and $\kappa^2 = (1/R^3)d(R^4\Omega^2)/dR$ is the square of the epicyclic frequency [11]. The growth rate of the MRI will thus decrease if the wavelength of the perturbation exceeds the size of the object, because the most prolific mode is filtered. If we associate the stellar radius with the maximum perturbation wavelength, $k = 2\pi/R_*$, we can obtain maximum magnetic fields for any set of ρ and $d\Omega^2/d \ln R$. This magnetic field pushing the maximum unstable growth beyond the size of the object is plotted in Fig. 3. The graph assumes the properties of an A0p star having a radius of $2.7R_\odot$ and a rotation period of say 10 days. The field strengths at the contours are in kG. Even if the initial differential rotation in the star is weak, the MRI may still be operating at its maximum growth rate if the magnetic fields do not exceed a few tens of kG. Surface magnetic fields of Ap stars rarely exceed 3.5 kG [12]. A dipolar field will thus rarely exceed 30 kG in the interior at $0.5R_*$.

The smaller size of the solar core compared with a A star envelope leads to smaller maximum magnetic field strengths as shown in Fig. 4.

The evolution of the differential rotation in a spherical shell is studied numerically. The initial angular velocity is defined by

$$\Omega = \frac{\text{Rm}}{\sqrt{1 + (2s)^{2q}}}, \quad (6)$$

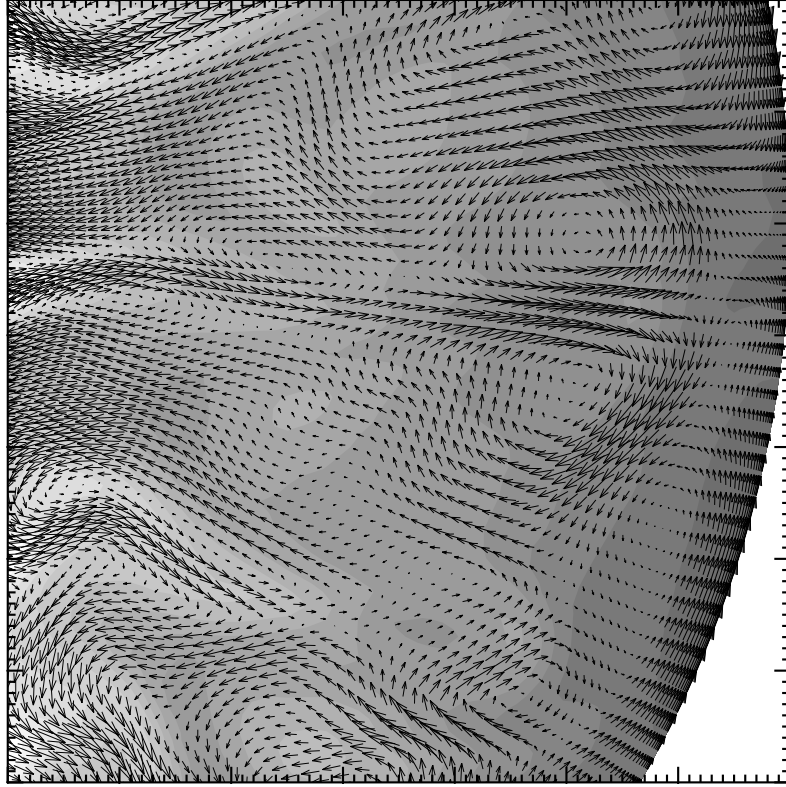


FIGURE 5. Vertical cut through the velocity field in the spherical computational domain. The gray shading represents the angular velocity, and the arrows are the meridional flow.

where $s = r \sin \theta$ is the axis distance and Rm is again the magnetic Reynolds number. This Rm will be varied in our simulations. The exponent q is always set to 2; it will later be used as a fitting parameter in order to obtain a measure for the steepness of the rotation profile. The initial magnetic field is composed of a homogeneous vertical field and a perturbation in a plane, with a wave vector parallel to the rotation axis,

$$\mathbf{B} = B_0[\hat{\mathbf{z}} + \varepsilon \sin(kz + \pi/4)\hat{\mathbf{x}}], \quad (7)$$

where $\hat{\mathbf{z}}$ is the unit vector in the direction of the rotation axis and $\hat{\mathbf{x}}$ is a unit vector in the equatorial plane. The wave number of the perturbation is $k = 4\pi$. We added $\pi/4$ to the second term in (7) in order to provide mixed parity to the system. Equatorial and axial symmetry are thus broken allowing the nonlinear system to develop flows and fields in all modes.

The system is evolved with 50 Chebyshev polynomials, 100 Legendre polynomials, and 30 Fourier modes. At magnetic Reynolds numbers as high as 10^4 , limited resolution may be a drawback of the simulations. The Legendre and Fourier energy spectra are therefore plotted in Figs. 7 and 8. While the contrast between the energies in the lowest and highest Fourier modes is at least 5 orders of magnitude, the contrast in the Legendre spectrum becomes as low as 100. The truncation is an issue for the flows near the rotation axis. The times for differential rotation decay are not altered by other spectral

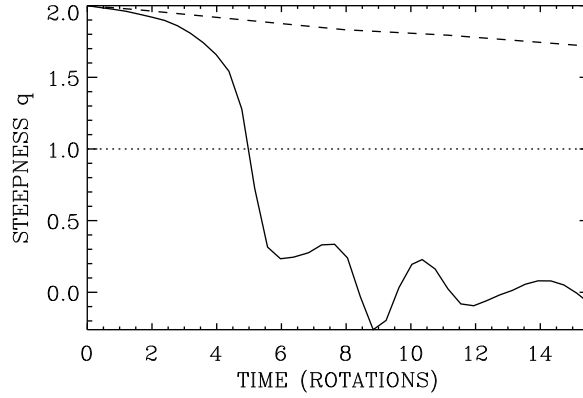


FIGURE 6. The evolution of the angular velocity gradient with time. What is called ‘steepness’ here is the value of q being the result of a fit of (6) with q and Rm as free parameters. Initially, $Rm = 10^4$, $Pm = 1$, and $Ra = 0$.

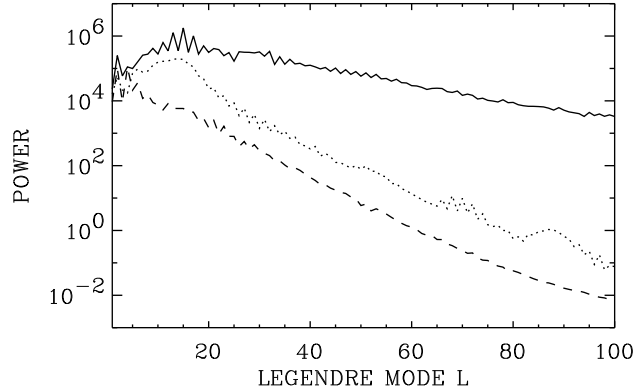


FIGURE 7. Spectrum of energy in the l -modes for $t = 0.001$ (dotted), $t = 0.003$ (solid), and $t = 0.01$ (dashed) diffusion times.

truncations; tests with only 50 Legendre polynomials led to the same decay time of differential rotation within 3%.

The flows emerging redistribute angular momentum and decrease the gradient in Ω . We measure the steepness of the rotation profile by fitting a function like (6) to the simulation data at a given instance. Rm and q are then free parameters; only the values of azimuthal averages of Ω in the equatorial plane are used for simplicity. The evolution of this q is shown in Fig. 6. The steepness decreases quickly on a time-scale of rotations and then varies around zero. For comparison, the purely viscous decay of the non-magnetic case is plotted as a dashed line. The initial Rm for this run was 10^4 , the other parameters were $Pm = 1$ and $Ra_\eta = 0$.

Stellar Reynolds numbers are much larger than 10^4 . Several runs were performed at various magnetic Reynolds numbers in order to get an extrapolated estimate for stellar

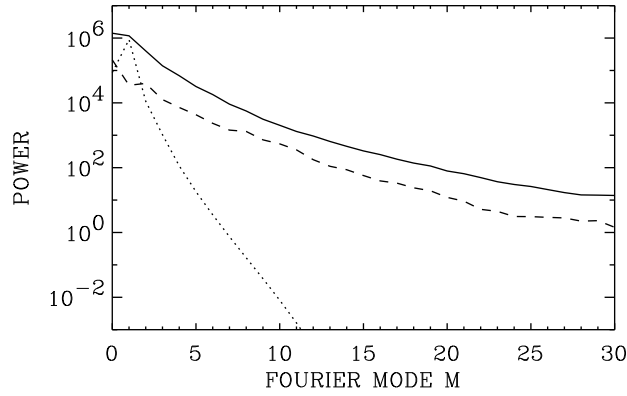


FIGURE 8. Spectrum of energy in the m -modes for $t = 0.001$ (dotted), $t = 0.003$ (solid), and $t = 0.01$ (dashed) diffusion times.

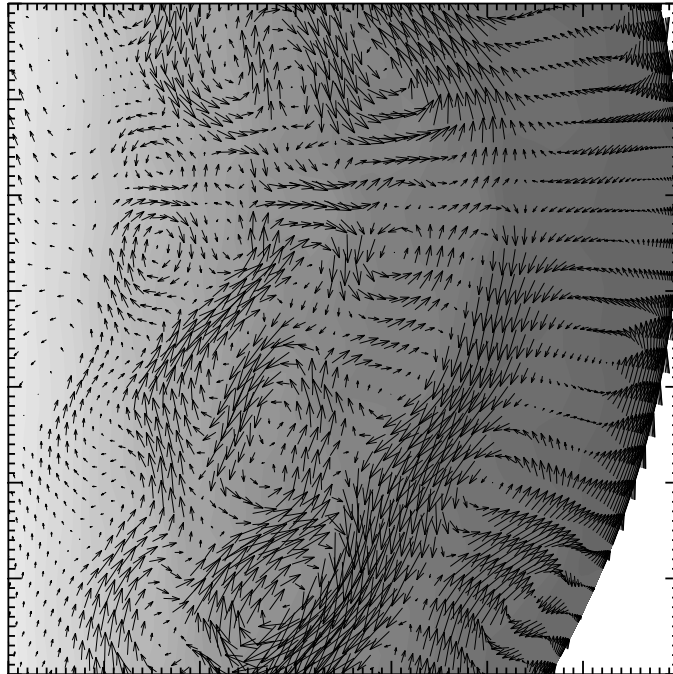


FIGURE 9. Vertical cut through the velocity field for a Rayleigh number of $Ra_\eta = -10^8$. Radial flows are suppressed as compared to the motions in Fig. 5.

conditions. As a result, the decay time amounts to roughly 10^7 – 10^8 yr. Since the age of the Sun is $5 \cdot 10^9$ yr, the process was fast enough to equalize differential rotation in the radiative core of the Sun. The more massive Ap stars have life-times of less than 10^9 yr. It is argued that the magnetorotational instability may be an ongoing process in the radiative envelopes of these stars.

Stellar radiative zones are very stably stratified. We can account for this by a negative

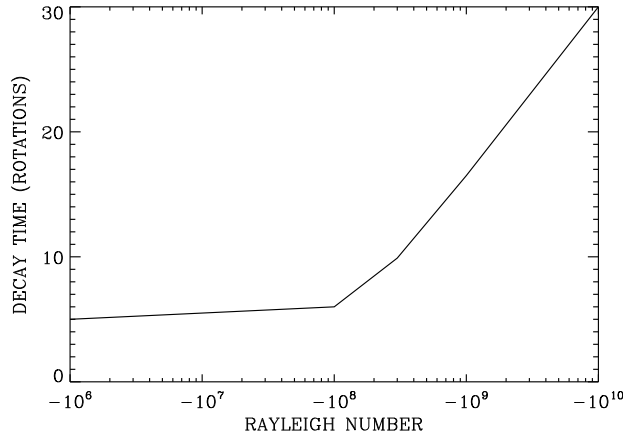


FIGURE 10. Decay time of differential rotation in dependence on the Rayleigh number. Strong subadiabaticity is on the right side. The computations were done with $Rm = 2 \cdot 10^4$.

Ra_η in the set of Eqs. (1)–(3). The negative buoyancy inhibits radial flows, and is expected to increase the decay time of differential rotation [13]. A snapshot of the velocity field at about the same time as in Fig. 5 is shown in Fig. 9. The decay time versus Ra_η is shown in Fig. 10. The MRI does not transport angular momentum radially anymore if Rayleigh numbers are beyond -10^{10} .

DYNAMO ACTION FROM LARGE-SCALE FLOWS

Differential rotation plus axisymmetric meridional circulations may provide a kinematic dynamo. The Cowling theorem says that the solution for the magnetic field must be non-axisymmetric, but no theorem exists saying that the flow must be non-axisymmetric. Dynamos from simple flows have been shown by various authors (see [14]). These might provide a dynamo mechanism for magnetic Ap stars lacking a solar convection zone as the driver of magnetic-field generation. The flows suggested by Eqs. 24–27 in [14] are capable of exciting a dynamo, but are they applicable to stellar radiative envelopes?

Following [2], the angular momentum transport by radiation is incorporated in the equation for u_ϕ as a forcing term. A flow with consistent differential rotation and meridional circulation can now be generated. The flow is shown in Fig. 11 and is used as constant velocity field for the induction equation which is studied exclusively in order to find the onset of dynamo action, that is the amplification of arbitrarily small magnetic fields.

No magnetic Reynolds number accessible to the code was able to excite a dynamo. Very high spectral truncation of 100 Chebyshev and 200 Legendre polynomials are used, and it is safe to say that no dynamo is found up to $Rm = 10^4$. Note that the meridional circulation being consistent with the differential rotation is in the opposite direction compared to what was used in [14]. We have thus made the test to reverse the radiation-induced circulation to come close to the case in [14]. Again, no dynamo action is found.

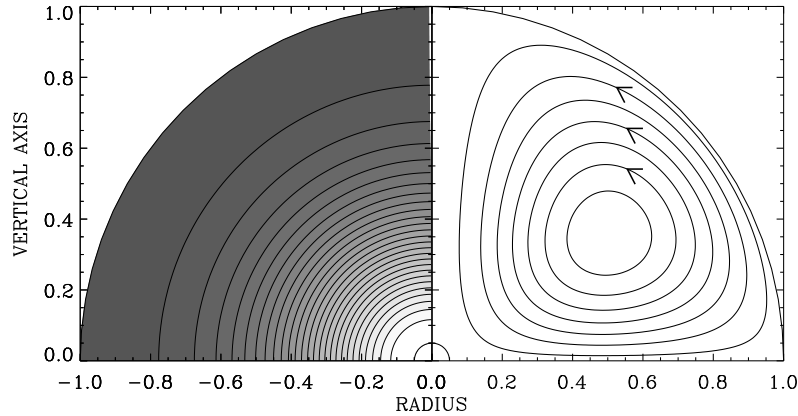


FIGURE 11. Consistent configuration of differential rotation and meridional circulation. The grey shading on the left side represents Ω -contours, the right side shows streamlines of the meridional circulation.

The result shows how subtle changes to the meridional circulation can be, deciding whether or not a dynamo is excited. It is concluded that a large-scale circulation dynamo is no likely explanation for the magnetic fields in Ap stars, and the fossil-field hypothesis is thus further supported.

ACKNOWLEDGMENTS

I am very grateful to Rainer Hollerbach for providing his numerical code and his help with it. I would also like to thank Aniket Sule for the computations of the solar tachocline.

REFERENCES

1. Charbonneau, P., Christensen-Dalsgaard, J., Henning, R., Larsen, R., Schou, J., Thompson, M., and Tomczyk, S., *ApJ*, **527**, 445–460 (1999).
2. Kippenhahn, R., *Zeitschr. f. Astrophys.*, **46**, 26–65 (1958).
3. Hollerbach, R., *Int. J. Num. Meth. Fluids*, **32**, 773 (2000).
4. Mestel, L., and Weiss, N., *Mon. Not. R. Astr. Soc.*, **226**, 123–135 (1987).
5. Rüdiger, G., and Kitchinov, L., *Astron. Nachr.*, **318**, 273 (1997).
6. McGregor, K., and Charbonneau, P., *Astrophys. J.*, **519**, 911 (1999).
7. Garaud, P., *Mon. Mot. R. Astron. Soc.*, **329**, 1–17 (2002).
8. Velikhov, E., *JETP*, **9**, 995 (1959).
9. Balbus, S., and Hawley, J., *ApJ*, **376**, 214–222 (1991).
10. Spitzer, L., *Physics of Fully Ionized Gases*, Interscience (2nd edition), 1962, New York, 1962.
11. Balbus, S., and Hawley, J., *Rev. Mod. Phys.*, **70**, 1–53 (1998).
12. Bychkov, V., Bychkova, L., and Madej, J., *A&A*, **407**, 631–642 (2003).
13. Balbus, S., and Hawley, J., *Mon. Not. R. Astron. Soc.*, **266**, 769 (1994).
14. Dudley, M., and James, R., *Proc. R. Soc. Lond. A*, **425**, 407–429 (1989).